Synthesis and Characterization of Mesostructured Titanium(IV) Fluorophosphates with a Semicrystalline Inorganic Framework

C. Serre,[†] M. Hervieu,[||] C. Magnier,[§] F. Taulelle,[‡] and G. Férey*[,†]

Institut Lavoisier, UMR CNRS 8637, Université de Versailles-St-Quentin-en-Yvelines, 45 Avenue des Etats-Unis, 78035 Versailles Cedex, France, Laboratoire RMN et Chimie du Solide, UMR CNRS 7510, Université Louis Pasteur, 4 Rue Blaise Pascal, 67070 Strasbourg, France, Rhodia, Centre de Recherches d'Aubervilliers, rue de la Haie Coq, 93308 Aubervilliers Cedex, France, and ISMRA, 6 Boulevard du Maréchal Juin, 14050 Caen, France

Received May 17, 2001. Revised Manuscript Received September 28, 2001

Hexagonal and lamellar mesostructured titanium(IV) fluorophosphates $[CH_3(CH_2)_nNR_3]_x$-$Ti_2OF_2H_{2-x}(PO_4)_2 \cdot 2H_2O$ ($x = 1, 2$; $n = 9-17$; R = CH_3, H) have been synthesized using aqueous solutions of titanium fluorophosphates and surfactants such as alkyltrimethylammoniumbromide or alkylamine. X-ray powder diffraction and HREM show that the hexagonal phase consists of arrays of hexagonal mesopores filled with surfactant. An extensive study of the synthesis conditions of the hexagonal CTAB phase was conducted with parameters such as the nature of the surfactant, concentrations of precursors, molar ratios, presence or absence of stirring, aging times, and temperature. Well-crystallized compounds appear only at low concentrations of surfactant and titanium, and the formation of the hexagonal phase occurs through the competitive complexation of titanium by fluorine and phosphates. It appears that the mesostructures form almost immediately at room temperature, whereas crystallization of the inorganic walls occurs only during hydrothermal aging. HREM, XRD, and solid-state NMR experiments confirm the existence of a semicrystalline order inside the inorganic framework. Removal of the surfactant by calcination of the hexagonal phase under nitrogen atmosphere leads to a mesoporous solid with semicrystalline pore walls exhibiting a surface area of over 400 m^2/g. A mechanism of formation is proposed on the basis of the TEM results, followed by a brief discussion concerning the mesostructured metallophosphates synthesized to date.

Introduction

Since 1992 and the initial publication by Kresge et al. at Mobil on the synthesis of various types of mesoporous silica,[1,2] many strategies have been developed to extend the composition of mesoporous materials to metal oxides other than silica.[3] Concerning catalysis, the production of pure mesoporous titanium dioxide, phosphate, or silicate would be very important for applications in acid, redox catalysis, or photocatalytic processes. The first approach to the synthesis of TiO_2 mesoporous compounds was developed, via an S^-I^+ route, by Antonelli et al.[4] The final product was not very stable and contained phosphates. Later, authors optimized this pathway for obtaining a pure but poorly organized mesoporous titanium dioxide.[5] Other groups have also recently developed neutral and ionic routes to the synthesis of mesoporous titanium oxophosphates exhibiting high specific areas with low organization and stability.[6] Ozin et al.[7] have established an original pathway for obtaining stable mesoporous titanium silicates via a nonaqueous route using glycometalates surfactants in ethylene glycol. Stable cubic mesoporous titanium dioxide with a low surface area was also reported by Stucky and co-workers,[8] using triblocks copolymers and $TiCl_4$ in ethanol as precursors.

However, all of these syntheses were conducted either in nonaqueous media or with expensive alkoxides. Our goal was to elaborate titanium-based mesoporous com-

* To whom correspondence should be addressed. E-mail: ferey@chimie.uvsq.fr.
[†] Université de Versailles-St-Quentin-en-Yvelines.
[‡] Université Louis Pasteur.
[§] Rhodia.
[||] ISMRA.

(1) Kresge, C. T.; Leonowicz, M. E.; Roth, W. J.; Vartuli, J. C.; Beck, J. S. *Nature* **1992**, *359*, 710.
(2) Beck, J. S.; Vartuli, J. C.; Roth, W. J.; Leonowicz, M. E.; Kresge, C. T.; Schmitt, K. T.; Chu, C. T.-W.; Olson, D. H.; Sheppard, E. W.; McCullen, S. B.; Higgins, J. B.; Schenker, J. L. *J. Am. Chem. Soc.* **1992**, *114*, 10834.
(3) (a) Corma, A. *Chem. Rev.* **1997**, *97*, 2373. (b) Ciesla, U.; Schüth, F. *Microporous Mesoporous Mater.* **1999**, *27*, 131.
(4) Antonelli, D. M.; Ying., J. Y. *Angew. Chem., Int. Ed. Engl.* **1995**, *34* (18), 2014.
(5) Antonelli, D. M. *Microporous Mesoporous Mater.* **1999**, *30*, 315.
(6) (a) Thieme, M.; Schüth, F. *Microporous Mesoporous Mater.* **1999**, *27*, 193. (b) Blanchard, J.; Schüth, F.; Trens, P.; Hudson, M. *Microporous Mesoporous Mater.* **2000**, *39*, 163. (c) Jones, D. J.; Aptel, G.; Brandhorst, M.; Jacquin, M.; Jiménez-Jiménez, J.; Jiménez-Lopez, A.; Maireles-Torres, P.; Piwonski, I.; Rodriguez-Castellon, E.; Zajac, J.; Roziere, J. *J. Mater. Chem.* **2000**, *10*, 1957.
(7) Khushalani, D.; Ozin, G. A.; Kuperman, A. *J. Mater. Chem.* **1999**, *9*, 1491.
(8) Yang., P. D.; Zhao, D. Y.; Margolese, D. I.; Chmelka, B. F.; Stucky, G. D. *Nature* **1998**, *396*, 152.

10.1021/cm0111276 CCC: $22.00
Published on Web 12/28/2001

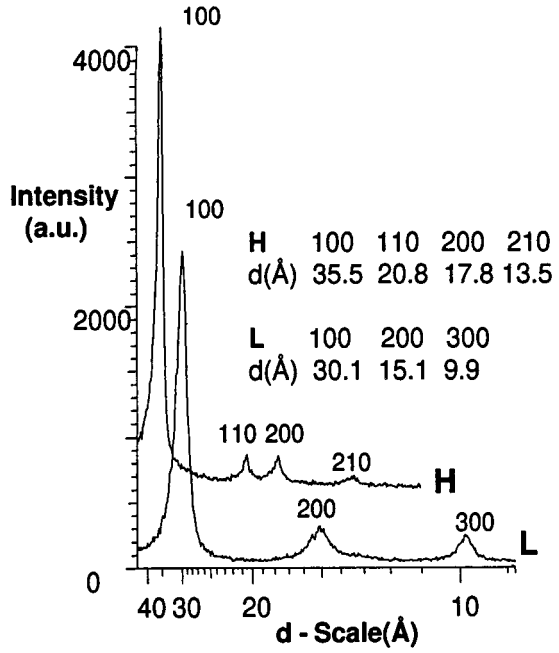

Figure 1. X-ray powder diffraction patterns of hexagonal (H) and lamellar (L) titanium fluorophosphates [synthesis conditions: TiF_4/10 H_3PO_4/0.3 S/360 H_2O (S = $C_{14}H_{29}N(CH_3)_3Br$ for H and $C_{14}H_{29}NH_3$ for L), aged for 48 h at 100 °C]. The Miller indices and the corresponding distances are also given.

pounds starting from inorganic titanium precursors in an aqueous medium. To avoid the precipitation of titanium dioxide, synthetic processes often use alkoxides precursors chelated with carboxylic groups[4] to prevent uncontrolled precipitation.[9] An alternative approach is to use nonaqueous solvents, but surfactants must have the capability of forming micelles, which is more difficult in these solvents than in water.[10] In addition, most of the nonsiliceous mesostructured materials that have been synthesized to date used conditions that mimic those of MCM-41 ("trial and error"),[11] and the rationalization of the synthesis conditions constitutes a major challenge for scientists interested in mesoporous compounds.

Our previous studies of the hydrothermal synthesis of titanium phosphates templated by organic molecules in fluorinated media[12] provided us with information concerning titanium fluorophosphate chemistry. The complexation of titanium by fluorine and phosphates is a competitive phenomenon, and titanium complexes exhibit both a high solubility in water and a high reactivity under hydrothermal conditions. We then transposed the synthesis conditions used previously for microporous solids to the production of mesostructured titanium fluorophosphates. Monoalkylamines or alkyltrimethylaminonium templates replaced the organic diamines previously used.

(9) Sanchez, C.; Livage, J. *New J. Chem*. **1990**, *14*, 513.

(10) Lindmann, B. Some Basic Aspects. In *Physics of Amphiphiles: Micelles, Vesicles and Emulsions: Proceedings of the International School of Physics, Enrico Fermi, Course Xc*; Degiorgio, V., Corti, M., Eds.; Società Italiana di Fisica: Bologna, Italy, 1984.

(11) (a) Sayari, A.; Liu, P. *Microporous Mater*. **1997**, *12*, 149. (b) Corma, A. Chem. Rev. **1997**, *97*, 2373. (c) Ying, J. Y.; Mehnert, C. P.; Wong, M. S. *Angew. Chem., Int. Ed*. **1999**, *38*, 56. (d) Ciesla, U.; Schuth, F. *Microporous and Mesoporous Mater*. **1999**, *27*, 131.

(12) Serre, C.; Ferey, G. *J. Mater. Chem*. **1999**, *9*, 579. (b) Serre, C.; Guillou, N.; Ferey, G. *J. Mater. Chem*. **1999**, *9*, 1185. (c) Serre, C.; Taulelle, F.; Ferey, G. *Chem. Mater*., in press.

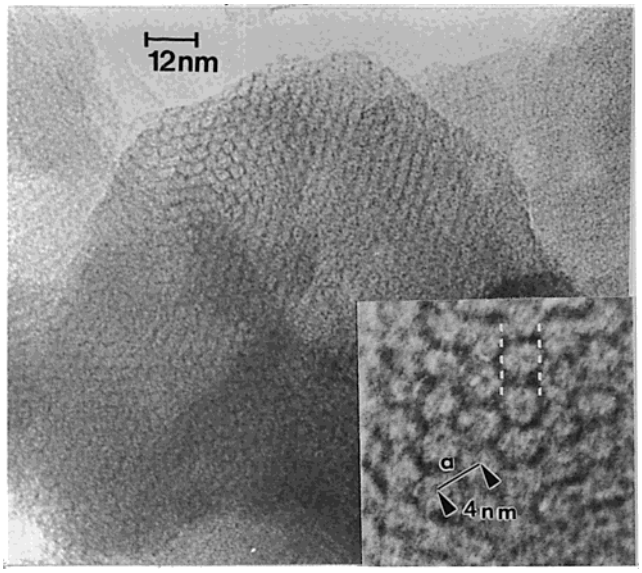

Figure 2. HREM micrographs of the hexagonal CTAB phase; an enlargement is included as an inset at the bottom left of the figure.

We report here the synthesis and characterization of the first mesostructured titanium(IV) fluorophosphates, with either hexagonal or lamellar structure, exhibiting a semicrystalline inorganic framework.

Experimental Section

Synthesis. The title compounds were synthesized using alkyltrimethylammoniumbromide $[CH_3(CH_2)_nN(CH_3)_3Br$ with $n = 9-17]$ for the hexagonal phases or tetradecylamine $[CH_3(CH_2)_{13}NH_2]$ for the lamellar solid. The Ti/F/H_3PO_4/surfactant/H_2O molar ratios were 1:3.5−8:1−20:0.15−1.0:120−400 for the hexagonal phases and 1:4:10:0.3−0.5:360 for the lamellar solids. In a typical sample preparation, 300 mg of TiF_4 (Aldrich, 99%) was dissolved in 4.65 mL of deionized water, and 1.65 ml of 85% H_3PO_4 (Prolabo) was added to the mixture. The surfactant solution, 200 mg of CTAB (Aldrich, 99%) in 8.7 mL of water, was introduced into the inorganic solution. The suspension was homogenized for times of between 30 s and 6 h. The suspensions were placed in a Teflon-lined digestive PARR bomb (23 mL) filled to 65% of its volume and heated at between 30 and 140 °C for different periods of time (12−168 h). The solids were then filtered, washed (water and acetone), and dried.

Analysis. Titanium, phosphorus, fluorine, carbon, nitrogen, and hydrogen contents were determined at the CNRS Central Laboratory of Analysis of Vernaison (69, France).

Physical Measurements. X-ray powder diffraction patterns were collected on a high-resolution ($\theta-2\theta$) Siemens D5000 diffractometer using λ_{Cu} Kα.

The electron diffraction studies were carried out with a JEOL 200CX electron microscope fitted with a tilting-rotating sample holder (tilt of ± 60°), and the high-resolution electron microscopy (HREM) experiments were performed with a TOPCON 002B microscope (point resolution of 1.8 Å). Both microscopes were equipped with energy dispersive spectroscopy (EDS) analyzers. Samples were prepared by dispersing the powder in alcohol and allowing the particles to deposit on a holey carbon film supported by a copper grid.

Solid-state NMR spectra were obtained using a DSX500 Bruker apparatus with an 11.7-T magnetic field and a 2-mm Teflon-headed MAS probe with a rotation speed of 20 kHz. ^{31}P spectra were recorded at 202.4156 MHz with a pulse time (P1) of 1.5 μs and a repetition time (D1) of 2 s; ^{19}F spectra were recorded at 470.4984 MHz with P1 = 2.5 μs and D1 = 2s. The reference samples were 85% H_3PO_4 (δ = 0 ppm) for ^{31}P and NaF (δ = 0 ppm) for ^{19}F.

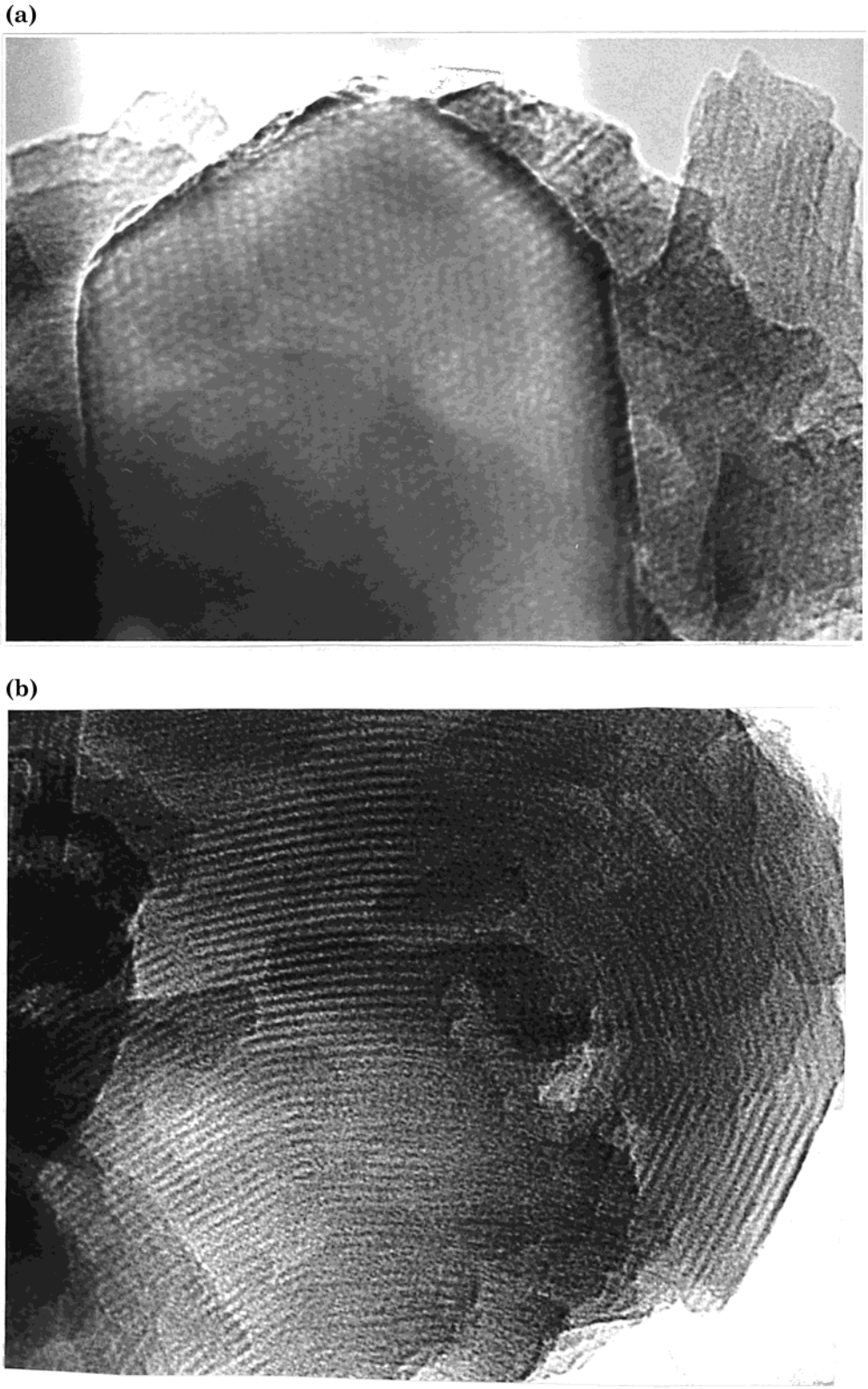

Figure 3. HREM micrographs of the hexagonal CTAB mesophase: (a) view parallel to the pores; (b) view perpendicular to the pores.

BET surface area measurements were conducted with an micromeretics ASAP 2010 apparatus using nitrogen (N_2) as the adsorbed gas.

Results and Discussion

Synthesis and Characterization. After the surfactant solution was added to the inorganic batch, a white precipitate immediately formed. After hydrothermal aging (2 days at 100 °C), well-crystallized mesostructured titanium fluorophosphates were obtained (Figure 1) with either lamellar or hexagonal structure depending on the nature of the surfactant used. Alkylamine surfactants (alkylammonium at pH < 1) led only to lamellar phases, whereas alkyltrimethylammoniumbro-

mide templates led to hexagonal solids. X-ray powder diffraction patterns showed (100), (110), (200), and (210) order for the hexagonal phase and (h00) (h > 3) reflections for the lamellar solid.

Quantitative analysis and TGA performed on the final compounds (aged 2 days at 100 °C) indicated approximate compositions of $[Ti_2(OH)F_2(PO_4)_2, S, xH_2O]$ (S for surfactant) for the hexagonal phases and $[Ti_2OF_2(PO_4)_2, S_2, xH_2O]$ for the lamellar solid.

Numerous particles of the CTA phases (aged at 100 °C) were characterized by a combination of ED, bright-field, and HREM imaging. The particles were platelet-shaped, about a few hundred nanometers wide. Large tilting showed that they were very thin with a mica-like character.

A typical HREM image shows a hexagonal phase with a honeycomb-like structure (Figure 2). The overall images indicate that the majority of the corresponding crystallites were also hexagonal-shaped, in agreement with the internal structure (Figure 3a). An enlarged image (inset of Figure 2) shows that the average periodicity of the close-packed spheroids is $a \approx 4$ nm. This value fits well with the X-ray diffraction data (intense reflection) a parameter (Figure 1). When tilted sufficiently, the structure exhibits a lamellar-type organization (Figure 3b); we attribute this to a perpendicular view of the hexagonal arrays observed previously (Figure 2) as others have reported such results with hexagonal mesostructures.[13]

Optimization of the Synthesis. To understand the synthesis process of the hexagonal solids, a study of the synthesis conditions was carried out. In the following, when no special comments are given, the product studied is the "final product", which means that it was stirred at room temperature, hydrothermally aged (100 °C), filtered, washed, and dried.

Nature of the Surfactant. The nature of the phase depends of the nature of the polar head of the surfactant. Small polar heads [alkylammonium ($-NH_3^+$) surfactant at pH < 1] lead to a lamellar phase, whereas larger polar heads [alkyltrimethylammonium ($-N(CH_3)_3^+$)] lead to hexagonal compounds. This is in agreement with the evolution of the packing parameter $\rho = V/a_o l_c$[14] (whereas V is the volume of the surfactant, a_o is the size of the polar head and l_c is the length of the alkyl chains). In addition, concerning the lamellar solid, no lamellar-to-hexagonal phase transformation was observed upon heating.

An increase in the size of the alkyl chain leads to an increase of the pore size for the hexagonal phases when the alkyl chains contain between 12 and 18 carbons. The crystallinity decreases rapidly for shorter chains.

Initial Stoichiometry. The CTA/Ti molar ratio was studied in three different ways: variable concentration of surfactant (S) at fixed concentration of Ti, fixed concentration of surfactant with variable concentration of Ti, and constant S/Ti ratio (0.3) with variable concentration. The crystallinity of the solids was estimated through the full width at half-maximum of the first reflection peak (100) of the X-ray patterns. It seems (Figure 4) that the synthesis of hexagonal phases requires both dilute surfactant and inorganic solutions with an optimized S/Ti ratio of 0.3. At higher concentrations, the crystallinity decreases rapidly, and in an excess of surfactant or inorganic species, either amorphous or liquid phases are obtained.

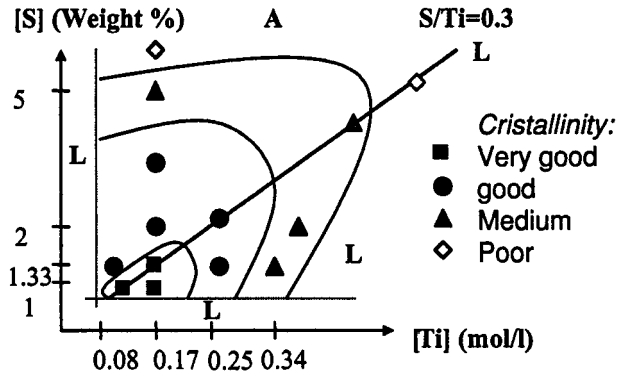

Figure 4. Surfactant/titanium concentration phase diagram in terms of crystallinity of the hexagonal CTAB solids. A, amorphous; L, liquid. [Synthesis conditions: TiF_4/10 H_3PO_4/xCTAB/$n H_2O$ (x = 0.1−1, n = 90−720), aged for 48 h at 100 °C.]

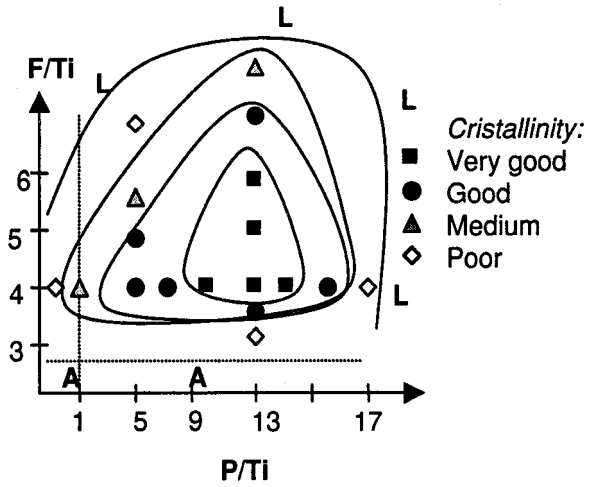

Figure 5. Fluorine/titanium and phosphorus/titanium ratios phase diagram in terms of crystallinity of the hexagonal CTAB solids. A, amorphous; L, liquid. [Synthesis conditions: TiF_4 + $x TiOCl_2/y H_3PO_4/x$CTAB/$n H_2O$ (x = 0−1, y = 1−25, n = 90−720), aged for 48 h at 100 °C.]

The F/Ti and P/Ti molar ratios were also modulated (Figure 5). The best results were obtained when excesses of both fluorine and phosphates are present, i.e., 4 < F/Ti < 8 and 9 < P/Ti < 14. At low fluorine content, the crystallinity decreases rapidly. At very high F/Ti and P/Ti ratios, no solids are obtained.

These results show that excesses of both fluorine and phosphates are needed to obtain crystalline solids. Thus, the competitive and strong anionic complexation of titanium by fluorine and phosphates is a key factor in the synthesis of these solids.

Influence of Aging. The F/Ti and P/Ti ratios were fixed at 4 and 10, respectively, and the titanium concentration was set at 0.17 mol/L. First, the influence of the room temperature stirring period was studied with an aging period of 48 h at 100°C. X-ray diffraction shows that

(13) (a) Chenite, A.; Lepage, Y.; Sayari, A. *Chem. Mater.* **1995**, *7*, 1015. (b) Yang, P. D.; Zhao, D. Y.; Margolese, D. I.; Chmelka, B. F.; Stucky, G. D. *Nature* **1998**, *396*, 152.

(14) Israelachvili, J. N. In *Physics of Amphiphiles: Micelles, Vesicles and Emulsions: Proceedings of the International School of Physics, Enrico Fermi, Course Xc*; Degiorgio, V., Corti, M., Eds.; Società Italiana di Fisica: Bologna, Italy, 1984.

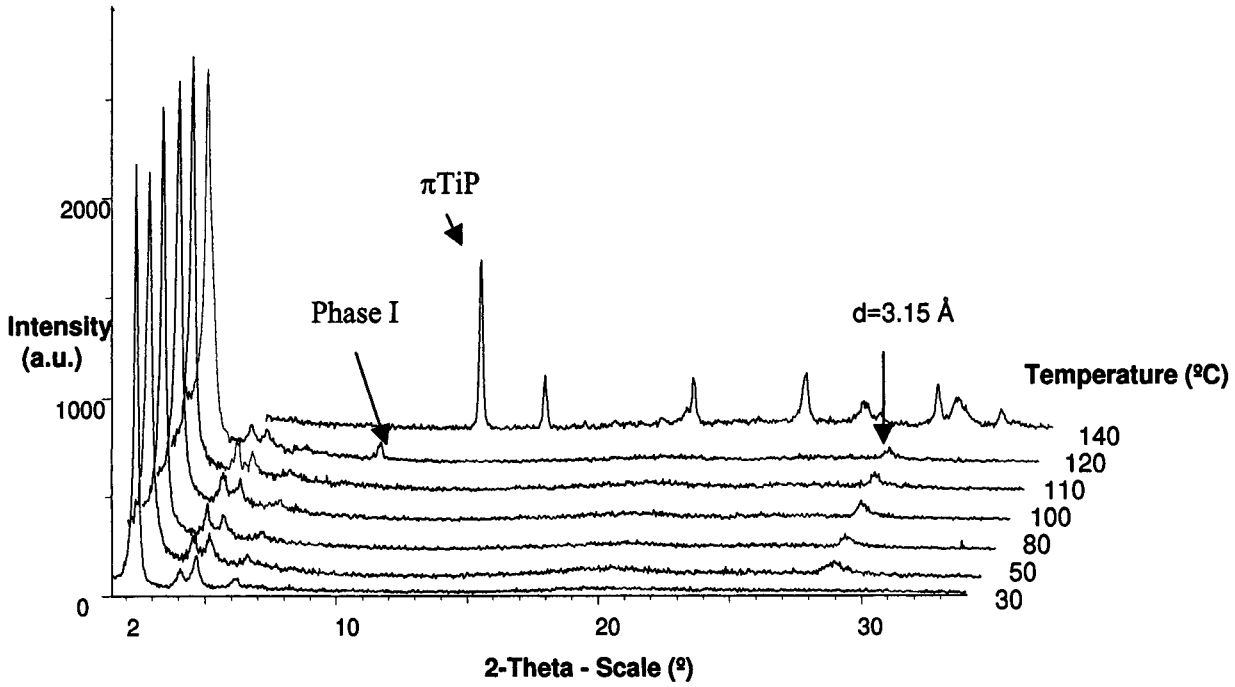

Figure 6. Influence of the aging temperature on the hexagonal CTAB solids (aged for 48 h at T = 25−140 °C). For a better understanding, a systematic 2θ offset of the patterns is applied.

the crystallinity decreased sharply if the stirring time exceeded 2 h.

Second, the stirring period was fixed (2 h), and the aging time was increased. The crystallinity and the pore size of the final product increased regularly, but after 4 days, poorly crystallized inorganic phases appeared.

Finally, the stirring and hydrothermal aging periods were both fixed (2 and 48 h, respectively), and the aging temperature was increased (Figure 6). Between 50 and 110 °C, the crystallinity increased smoothly, and an additional reflection at 3.15 Å appeared (Figure 6). A further increase in the temperature (120−140 °C) leads to the progressive destabilization of the mesostructured phase at the benefit of the growth inorganic phases. A first solid, denoted phase I, appears at 120 °C, and the titanium phosphate labeled πTiP,[15] is present at 140 °C. Other studies have shown that phase I is a precursor of πTiP.[16]

Study of the Crystallinity of the Inorganic Walls. The 3.15-Å reflection observed previously could correspond to an unknown byproduct. However, its growth and shape are correlated with those of the mesostructured solids; thus, we propose that this peak is due to an organization inside the inorganic walls that appears during aging. To test this hypothesis, an ED study was performed on particles exhibiting extended oriented domains (Figure 7a). A pattern recorded after the above particle was tilted is given in Figure 7b. Along the channels (direction $d_{\perp}$), a diffuse streaky line is observed that arise from the imperfect arrangement of the channels and the lamellar shape of the crystal. Along the channels (direction d_w), the inter-reticular distances are 3.15 Å (intense node) and 6.3 Å (weak intermediate node). Another example is observed in Figure 7c, with a local periodicity along the direction parallel to the channels of 12.6 Å (= 4 × 3.15 Å). These results correspond very well with the X-ray data (Figure 6) and undoubtedly show that the pore walls are organized. In fact, according to the HREM results (Figure 3), the characteristic distances are much higher along the direction parallel to the pores (c axis) and allow for X-ray diffraction in this direction (c axis). In the direction perpendicular to the pores, the thickness of the walls is not large enough (∼10−12 Å) to produce any diffraction pattern. This 3.15-Å order probably corresponds to the Ti−P interatomic distance, and the presence of −(Ti−O−P)− chains along the c axis within the framework .

Solid-state ^{19}F and ^{31}P NMR spectra were recorded before and after hydrothermal aging (Figure 8). Before the thermal treatment, no ^{19}F signal can be observed, and very broad peaks are present in the ^{31}P spectrum. After aging, one broad ^{19}F peak around +10 ppm and three ^{31}P peaks at −13, −25, and −30 ppm are observed. These results confirm that a crystalline order within the inorganic walls appears through aging.

In addition, ^{19}F liquid NMR studies[16] indicate that shifts of about +10 ppm likely correspond to $TiOF^+$ species; in our case, this suggests that fluorine atoms are in terminal positions and are probably interacting with the positively charged heads of the surfactants. This would explain the broadness of the observed ^{19}F peak because of the disorder inside the micelles. Considering values reported previously for other titanium phosphates (e.g., αTiP and γTiP) at −12, −25, and −30 ppm, our ^{31}P NMR peaks could be assigned, respectively, to Q2, Q4, and Q4 metal−phosphorus connectivities. However, other titanium phosphates, such as ρTiP and πTiP that possess only Q4 phosphorus,[15,16] exhibit values of around −11 and −25 ppm. Thus, no assignment is proposed for the ^{31}P NMR peaks.

(15) Bortun, A. I.; Khainakov, S. A.; Bortun, L. N.; Poojary, D. M.; Rodriguez, J.; Garcia, J. R.; Clearfield, A. *Chem. Mater.* **1997**, *9*, 1805.
(16) Serre, C.; Lorentz, C.; Taulelle, F.; Ferey, G. Unpublished results, 1999.

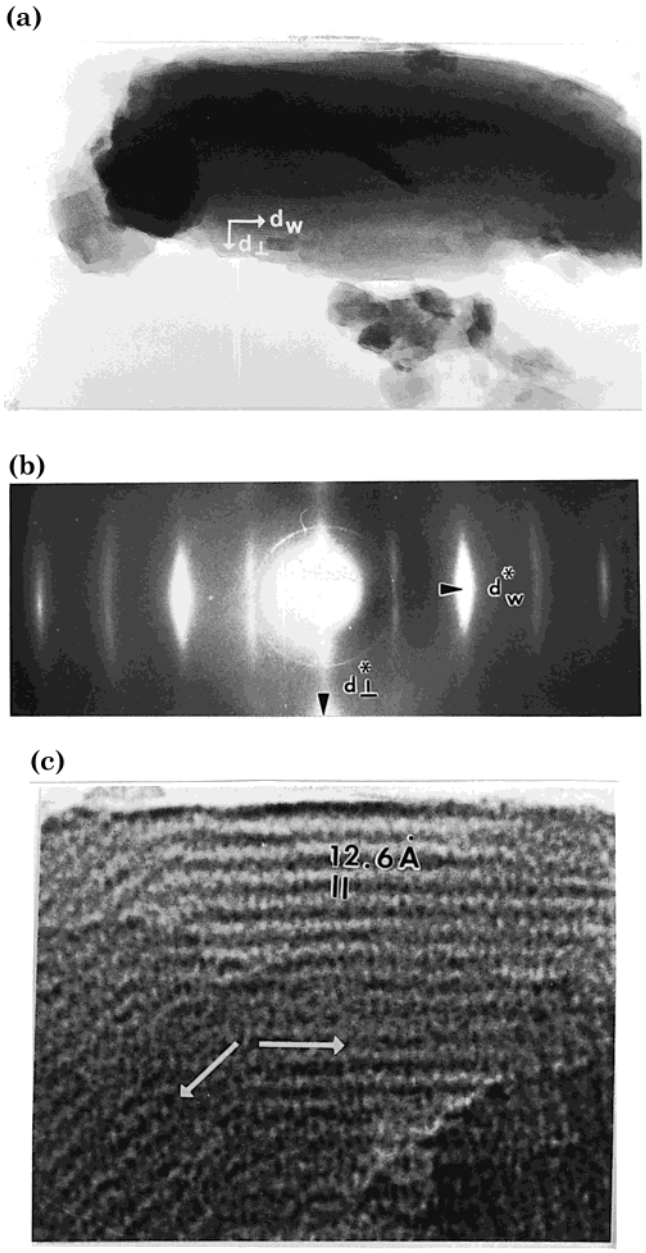

Figure 7. (a) General view by HREM of a hexagonal CTA particle. (b) ED pattern of the above particle. (c) Enlarged HREM micrograph of the above particle.

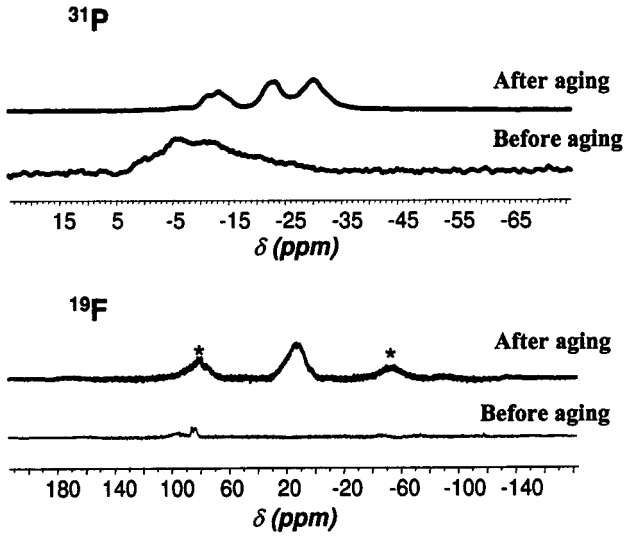

Figure 8. Solid-state ^{31}P and ^{19}F NMR spectra of hexagonal CTAB solids before and after hydrothermal aging for 2 days at 100 °C. (*) rotation bands.

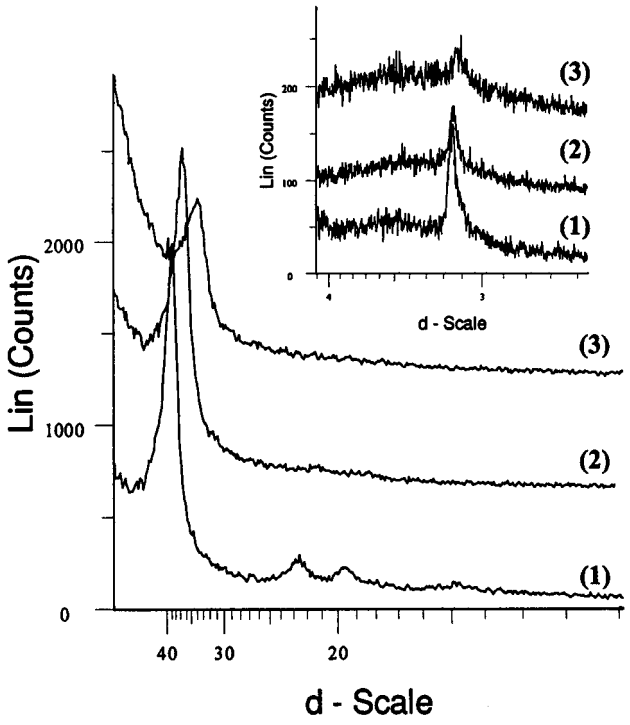

Figure 9. X-ray powder diffraction pattern of hexagonal CTAB phases: (1) as-synthesized, (2) calcined for 2 h at 350 °C under nitrogen, (3) calcined for 2 h under nitrogen and for 16 h under air at 350 °C. An inset representing the high-angle section of the X-ray diffraction patterns of the above solids is located at the top of the figure. d-scale is in Angströms

Thermal Behavior. The surfactant removal of the hexagonal CTAB solids was also studied.

When the surfactant was removed directly by thermal treatment under air, the structure collapsed completely. To soften the thermal treatment, a calcination treatment under N_2 atmosphere (2 h at 350 °C) was performed. X-ray powder diffraction indicates that a loss of mesoscopic order and a pore contraction of 2 Å occurred (Figure 9). As the calcined solid still contains traces of carbon (2−3%), a second calcination under air at 350 °C was performed overnight. This led to a decrease in intensity of the (100) peak and an additional pore contraction of 3 Å. The final carbon-free mesoporous solid exhibited a broad peak at $d \approx 34$ Å (Figure 9), and high-angle X-ray scattering revealed that the 3.15-Å peak characteristic of the crystallinity of the pore walls was still present, despite a decrease in its intensity (Figure 9). The corresponding specific surface areas of the calcined products were 330 m^2/g after the nitrogen treatment and 410 m^2/g after the second treatment. A narrow hysteresis loop was observed for the N_2 adsorption−desorption nitrogen isotherm, and the corresponding BJH calculation gave a broad pore size distribution centered at 22 Å (Figure 10). Other methods are currently under study in an effort to further optimize the surfactant removal process.

Approach of the Formation Mechanism. In the course of the TEM investigation, different structural organizations were observed that suggested a possible mechanistic pathway for the last step of formation of

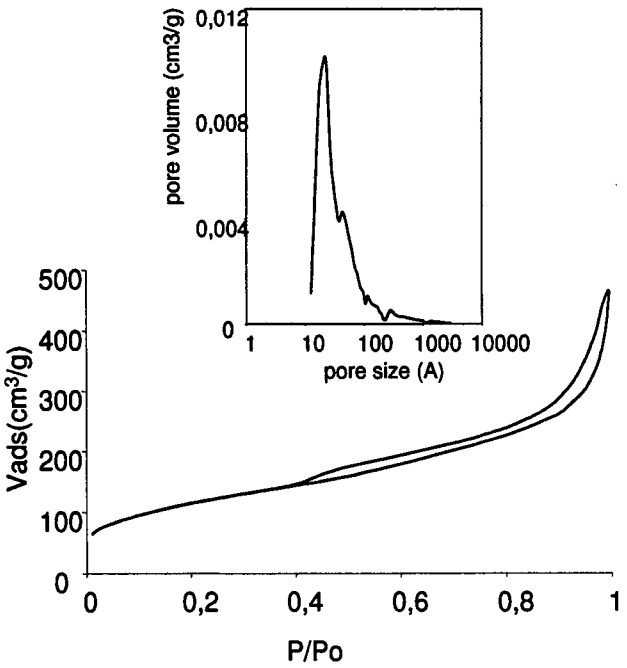

Figure 10. Nitrogen adsorption isotherm of a hexagonal CTAB mesostructured solid calcined for 2 h under nitrogen and for 16 h under air at 350 °C. The BJH pore distribution calculation is represented as an inset at the top of the figure.

the hexagonal phase and its evolution under annealing. The initial formation of the mesotextured solid starting from surfactant moieties and inorganic species is not discussed in this section.

The starting point of our structural mechanism appears to be a hexagonal arrangement of close-packed, faceted spheroids. A typical HREM image is shown in Figure 2. The crystallites are hexagonal-shaped, and the number of layers of spheroids in the perpendicular direction is small. At this stage, the perfect hexagonal arrangement of the spheroids is not always followed. Deviations are even visible in the hexagonal crystallites (Figure 2). Such effects are assumed to be favored by the flexibility of the spheroid inner walls and correlated with the beginnings of the second step of the transformation in which the hexagonal array of the spheroids is destroyed. An example of a particle that exhibits this evolution is shown in Figure 11. The wall between two face-sharing spheroids is broken, forming a large double unit (see the two black arrows in Figure 11) or triple unit. The mechanism spreads toward the outside of the grain. At this step, therefore, the particles are built up from a small core of a hexagonal array of a few faceted spheroids, surrounded by the new structural multiple units (see Figure 12). These units can be described as the results of a spheroid clustering, and they become longer as the internal walls are broken. The "opening" of the internal walls occurs along the equivalent [110] directions of the hexagonal system and up to the formation of curved channels.

The particles are then formed of concentric circular channels. This is exemplified in the overall image (curved line in the inset) and enlarged image in Figure 12. Note, by the way, that the average inner diameter of the channels remains directly related to the "interreticular" distances of the hexagonal pristine array, i.e., close to 3.5 nm (see white dotted line in the inset of Figure 2). The concentric arrangement of the curved channels implies a great flexibility of the bonds forming the walls.

As the last spheroids of the hexagonal core are opened, the channels straighten, forming first small oriented domains (see scheme in Figure 13 and arrows in inset of Figure 12 and in Figure 7c). These small regions progressively disappear, so that the particles are finally formed of more and more extended domains. Note that no specific value was observed for the angles between the oriented domains. This can be explained by the flexibility of the framework. The particle shown in Figure 7a is composed of a single domain with straight parallel channels, 35.5 Å apart.

The average diameter of the channels remains roughly constant in all of these transformations. The inter-

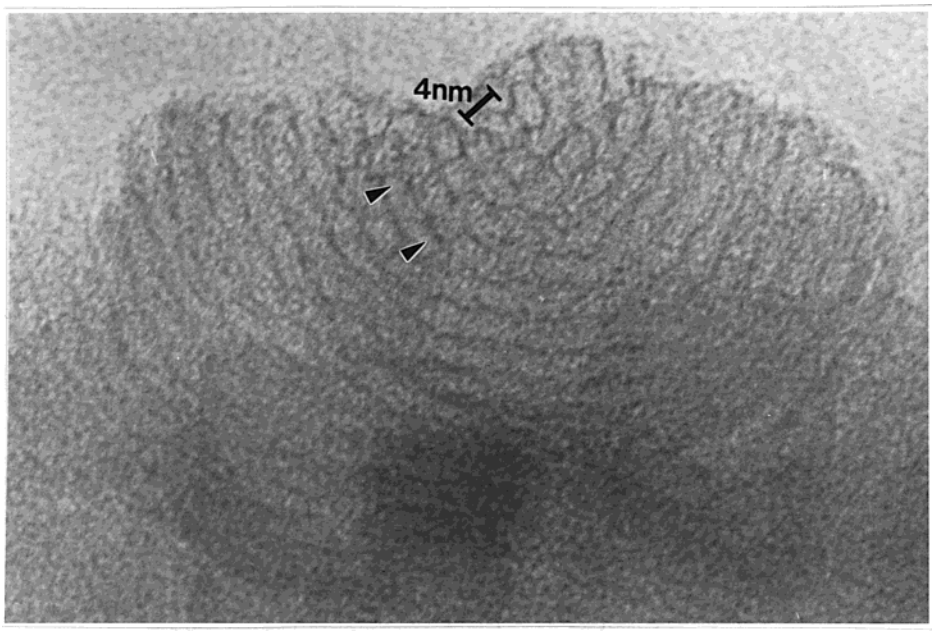

Figure 11. HREM micrograph of a hexagonal CTA particle exhibiting the beginning of wall destruction.

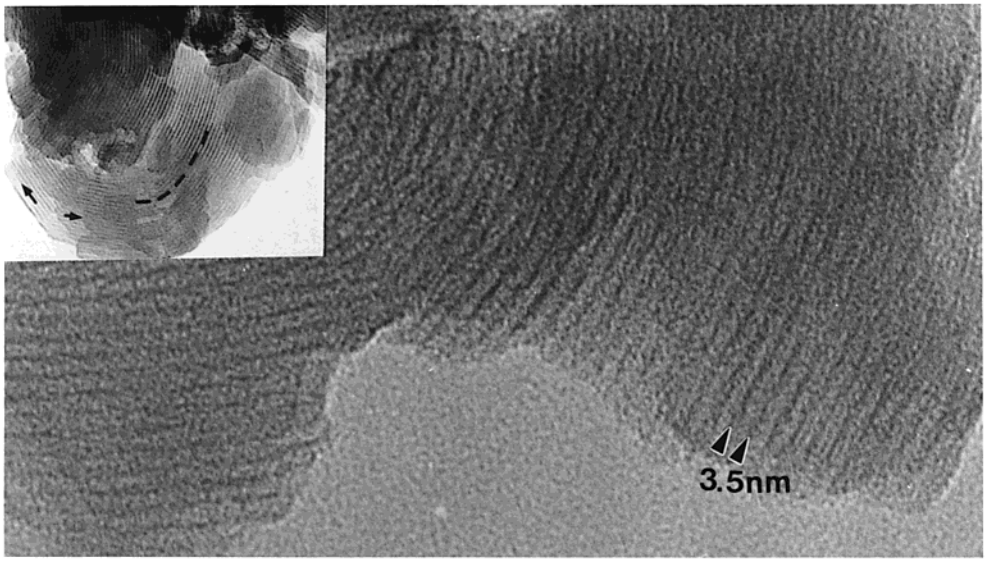

Figure 12. HREM micrograph of a hexagonal CTA particle with circular concentric channels; an enlargement is presented in an inset at the top right of the figure.

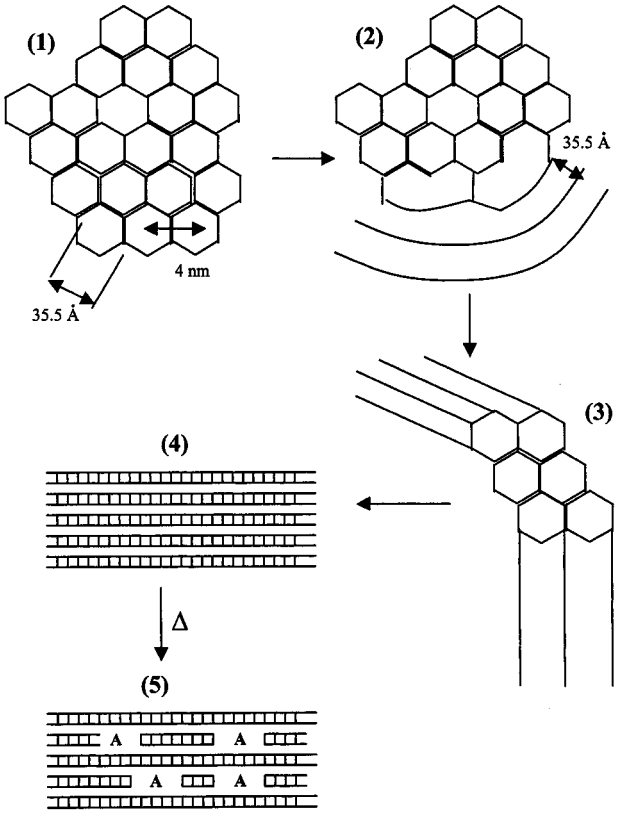

Figure 13. Proposed scheme for the formation mechanism of the hexagonal CTA solid and its evolution under annealing. Step 1, formation of faceted hexagonal spheroids. Step 2, agglomeration of spheroids, followed by a partial wall destruction, and a propagation of the internal wall opening along the [110] direction and formation of concentric channels. Step 3, straightening of the channels leading to small oriented domains. Step 4, formation of extended oriented domains with regular inter-reticular distances upon further straightening. Step 5, progressive destruction of the organization under annealing (at 350 °C under nitrogen).

reticular distance $d = 35.5$ Å is therefore common to all of the intermediate structures. This can explain the high intensity of the corresponding peak in the X-ray diffraction pattern with respect to the other peaks.

One of the consequences of the channel straightening is the stabilization of regular interatomic distances in the walls (direction denoted by d_w in Figure 7a), at variance to what happens in curved walls (Figure 12). This is clearly observed in both the ED patterns and the HREM images, and the periodic organization in the direction parallel to the pores with the characteristic 3.15-Å distance appears (Figure 7c). This is in agreement with the XRD and solid-state NMR results.

In the annealed sample (calcined at 350 °C under N_2), channel wall destruction is occurring (see the white arrow in Figure 14). The earlier existence of channels in the pristine sample is still visible, but clearly, some amorphous areas are appearing (see area denoted A in Figure 14). This could explain why the surface areas of the calcined samples are not very high.

Finally, the main transitions are presented in Figure 13. The faceted spheroids are drawn in the form of hexagons in Figure 13 for simplicity. However, because the study was performed on products after aging, a complete study of the formation mechanism at each stage of the synthesis is needed.

Comparison with Other Mesostructured Metallophosphates. Most mesoporous oxophosphates compounds synthesized to date, except for a stable mesoporous aluminophosphate,[17] use phosphatation as a postsynthesis treatment to stabilize the framework before calcination. In other cases,[6] phosphates are mixed with the surfactant prior to addition with the metal precursors. Thus, no reproducible phosphorus/metal ratio in the final solids is obtained. In our case, the prior complexation of titanium by phosphates and fluorine anions gives a reproducible distribution of species in the inorganic solutions. Quantitative analysis was performed on the final hexagonal CTAB solids synthesized with variable P/Ti initial ratios (other ratios fixed). It appears that the composition of the solid is unchanged (P/Ti = F/Ti = 1, S/Ti = 0.5) and does not depend on the initial ratios in the solution. Thus, according to the

(17) Perez, J. O.; Borade, R. B.; Clearfield, A. *J. Mol. Struct.* **1998**, *470*, 221.

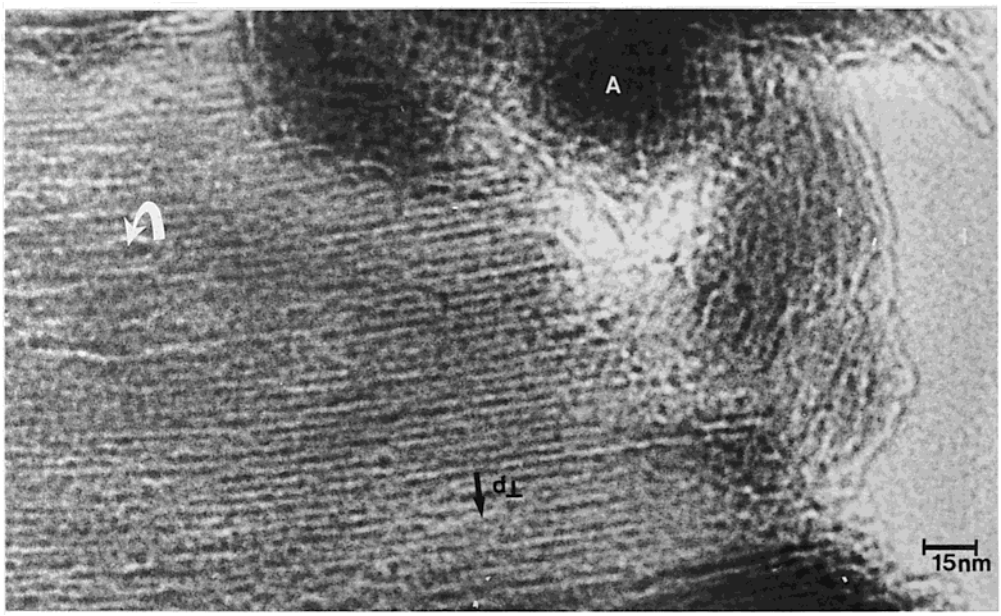

Figure 14. HREM micrograph of a hexagonal CTA particle calcined for 2 h at 350 °C under nitrogen. A, amorphous area.

concept of charge density matching developed by Stucky and co-workers,[18] only the right inorganic species present in the early stages of the synthesis react with surfactant aggregates (or monomers) to produce the mesostructured compounds. Recently, similar approaches were developed with vanadium phosphates;[19] either the oxidation state of vanadium or the pH was changed to modulate the nature of the species in solution, and well-crystallized, but thermally unstable, mesotextured solids with a controlled P/V stoichiometry were obtained.

Conclusion

We report here a pathway for the synthesis of hexagonal (or lamellar) mesostructured titanium-based compounds with controlled phosphorus and fluorine contents starting from inorganic precursors in an aqueous medium. A study of the synthesis of the hexagonal phase revealed that the crystallization of mesostructured solids occurs through the competitive complexation of titanium by fluorine and phosphates. TEM, NMR, and XRD measurements also showed that, if the mesostructure appears at the first steps of the synthesis at room temperature, then hydrothermal aging leads to an unusual crystallization of the inorganic pore walls with a characteristic 3.15-Å interatomic distance.

Removal of the surfactant by a soft two-step calcination treatment leads to an organized porous solid with a relatively high surface area and an unusual pore wall crystallinity.

TEM results also allowed us to propose the steps of a mechanism of organization within the solid starting from hexagonally close-packed spheroids and leading to extended oriented particles with a periodicity in the inorganic framework.

Finally, the next steps in this research involve the NMR study of the formation mechanism of the hexagonal phase and the extension of this synthetic pathway to other tetravalent systems; initial results will be published soon elsewhere.[16,20]

Acknowledgment. C. Lorentz (Laboratoire Chimie et RMN du solide, Universite Louis Pasteur, Strasbourg, France) is gratefully acknowledged for her collaboration. We gratefully acknowledge Rhodia for its financial support.

CM0111276

(18) Huo, Q.; Margolese, D. I.; Ciesla, U.; Feng, P.; Gler, T. E.; Sieger, P.; Leon, R.; Petroff, P.; Schuth, F.; Stucky, G. D. *Nature* **1994**, *368*, 317.

(19) (a) El Haskouri, J.; Roca, M.; Cabrera, S.; Bertran-Polter, M.; Beltran-Porter, D.; Marcos, M. D.; Amoros, P.; *Chem. Mater.* **1999**, *11*, 1446. (b) Mizuno, N.; Hatayama, H.; Uchida, S.; Tagushi, A., *Chem. Mater.* **2001**, *13*, 179.

(20) Serre, C.; Auroux, A.; Gervasini, A.; Hervieu, M.; Férey, G. *Angew. Chem., Int. Ed.*, manuscript submitted.